Yang et al. Nanoscale Research Letters (2016) 11:283
DOI 10.1186/s11671-016-1492-8

Nanoscale Research Letters

NANO EXPRESS Open Access

Plasmonic Pd Nanoparticle- and Plasmonic Pd Nanorod-Decorated $BiVO_4$ Electrodes with Enhanced Photoelectrochemical Water Splitting Efficiency Across Visible-NIR Region

Weiwei Yang[1,2,3], Yunjie Xiong[1,2,3], Liangliang Zou[1], Zhiqing Zou[1*], Dongdong Li[1], Qixi Mi[3], Yanshan Wang[1] and Hui Yang[1,2*]

Abstract

The photoelectrochemical (PEC) water splitting performance of $BiVO_4$ is partially hindered by insufficient photoresponse in the spectral region with energy below the band gap. Here, we demonstrate that the PEC water splitting efficiency of $BiVO_4$ electrodes can be effectively enhanced by decorating Pd nanoparticles (NPs) and nanorods (NRs). The results indicate that the Pd NPs and NRs with different surface plasmon resonance (SPR) features delivered an enhanced PEC water splitting performance in the visible and near-infrared (NIR) regions, respectively. Considering that there is barely no absorption overlap between Pd nanostructures and $BiVO_4$ and the finite-difference time domain (FDTD) simulation indicating there are substantial energetic hot electrons in the vicinity of Pd nanostructures, the enhanced PEC performance of Pd NP-decorated $BiVO_4$ and Pd NR-decorated $BiVO_4$ could both benefit from the hot electron injection mechanism instead of the plasmon resonance energy transfer process. Moreover, a combination of Pd NPs and NRs decorated on the $BiVO_4$ electrodes leads to a broad-band enhancement across visible-NIR region.

Keywords: Plasmonic Pd, $BiVO_4$, Photoelectrochemical water splitting, Surface plasmon resonance

Background

Solar hydrogen generation through photoelectrochemical (PEC) water splitting offers an efficient and sustainable solution to the global energy problem [1–5]. Recently, $BiVO_4$ has emerged as a promising material for PEC water splitting due to its photoactivity in visible light region [6]. However, $BiVO_4$ photoanodes suffer from rapid charge carrier recombination, slow water oxidation kinetics, and insufficient photoresponse in the spectral region with energy below the band gap of 2.4 eV [6], which limit its water splitting efficiency. Therefore, strategies such as doping [7–12], nanostructuring [13–18], and loading of oxygen evolution catalysts (OECs) [7, 9, 19, 20] have been adopted to improve the water splitting efficiency of $BiVO_4$.

As reported, several dopants, such as W, Mo, and P, are reported to improve the PEC performance of $BiVO_4$ [7–12]. Doped $BiVO_4$ exhibits the improved carrier density, enhanced conductivity, or even increased hole diffusion length, thus resulting in enhanced PEC properties. Furthermore, the short diffusion length of photoexcited charge carriers is the main reason for the dominant electron-hole recombination in the bulk of $BiVO_4$. To address this issue, the diffusion length for charge carriers can be shortened by nanostructuring, thereby reducing bulk recombination [13–18]. To increase the water oxidation kinetics, research efforts have been placed on the loading of the OECs on $BiVO_4$ [7, 9, 19, 20]. Among these OECs, the Co-Pi and FeOOH catalysts can lead to a negative-shift of onset potentials of water oxidation and effectively enhance the magnitude of photocurrent [7, 9, 19]. However, through these strategies, the enhanced photoactivity of $BiVO_4$ has only been achieved in the spectral region with energy above the band gap. To improve the PEC water splitting efficiency of $BiVO_4$ in the spectral

* Correspondence: zouzq@sari.ac.cn; yangh@sari.ac.cn
[1]Shanghai Advanced Research Institute, Chinese Academy of Sciences, Shanghai 201210, China
Full list of author information is available at the end of the article

region with energy below the band gap or even in the near-infrared (NIR) region, whose energy accounts for 56.3 % of that of the solar spectrum [21], still remains a big challenge.

Recently, a new approach involving metal nanostructures in enhancing the photoactivity of TiO_2 in the spectral region with energy below the band gap via plasmonic effect has received much attention [22–24]. Surface plasmon resonance (SPR) is an intrinsic property of metal nanostructures, in which the oscillation frequency is highly sensitive to their shape and size of the metal nanostructures as well as the dielectric constant of the surrounding environment [25–30]. The plasmonic metal nanostructures localize the optical energy by SPR and enhance the photoactivity of semiconductors through either near-field electromagnetic enhancement or hot electron injection [22–24]. For example, Hsu et al. reported that the performance of Au nanostructure-decorated TiO_2 nanowires for PEC water splitting was enhanced across entire UV-visible region [23]. Although an enhancement in the PEC water splitting efficiency was also observed on $BiVO_4$ electrodes with plasmonic metal nanostructures, such as Au and Ag [31–33], there are no reports that the photoactivity of $BiVO_4$ can be improved in the spectral region with energy below the band gap or even in the NIR region by exploiting plasmonic metal nanostructures.

This work reports that the enhancement of PEC water splitting efficiency can be effectively extended into the visible-NIR region by the combination of Pd nanoparticles (NPs) and nanorods (NRs) with $BiVO_4$ electrodes. The mechanisms of activity enhancement both in the visible and NIR regions have been discussed.

Methods

Preparation of $BiVO_4$ Electrodes

The $BiVO_4$ electrodes were prepared as previously reported procedure [19]. Solutions for electrodeposition were prepared by dissolving 10 mM $Bi(NO_3)_3$ (98 %, Alfa Aesar) in a solution of 35 mM $VOSO_4$ (97 %, Sigma Aldrich) at pH < 0.5 with HNO_3 (65 %, Acros Organics). Then 2 M CH_3COONa (≥99.0 %, Alfa Aesar) was added, raising the pH to ~5.1, which was then adjusted to pH 4.7 with a few drops of HNO_3. Acetate serves to stabilize other insoluble Bi (III) ions at pH 4.7. This mildly acidic pH condition must be used because at pH lower than 2 where Bi(III) is soluble, no film can be formed while at pH higher than 5, V (IV) precipitates from solution. A three-electrode cell was used for electrodeposition, with an fluorine-doped tin oxide (FTO, 8 Ω/□, Hartford Glass Co.) coated glass substrate as working electrode, a Ag/AgCl (4 M KCl) as reference electrode and a platinum foil as counter electrode. A potentiostat (Sloartron SI 1287) was used for electrodeposition. Deposition of amorphous Bi–V–O films was carried out potentiostatically at 1.9 V vs Ag/AgCl (4 M KCl) for 5 min at 70 °C (ca. 2 mA cm^{-2}). The as-deposited films were converted to crystalline $BiVO_4$ and amorphous V_2O_5 by annealing at 500 °C for 1 h in air, and pure $BiVO_4$ was achieved by dissolving the V_2O_5 in 1 M KOH under stirring for 20 min.

Synthesis of Pd NPs and NRs

A simple but very efficient method that uses CO as reducing agent to synthesize Pd NPs and NRs has been developed and will be reported elsewhere. In brief, before the synthesis, 80 mM/L NaCl (≥99.0 %, Sigma Aldrich) and 40 mM/L $PdCl_2$ (≥99.9 %, Sigma Aldrich) was dissolved in 50 mL CH_3OH (≥99.9 %, Sigma Aldrich) to form Na_2PdCl_4 for preparation. Then, a flask was added 210-mg polyvinylpyrrolidone (K 30, average Mw 40,000, Sigma Aldrich) and 100 mL of 3.876 mM Na_2PdCl_4. To produce Pd NRs or NPs, 0.2- or 4.0-mL ultra-purity water (Millipore Milli-Q purification system, resistivity >18 MΩ cm) was added respectively. High-purity N_2 with a flow rate of 200 mL/min was used for deaeration of the solution for 1 h under intense stirring. Then, high-purity CO with a flow rate of 200 mL/min was introduced to the flask under gentle stirring for 10 min. After that, a common balloon linked to the flask was blown up with CO to keep the reducing atmosphere for 4 h. During the whole synthesis process, the reaction system was keep at 30 °C.

Preparation of Pd Nanostructure-Decorated $BiVO_4$ Electrodes

Pd nanostructure-decorated $BiVO_4$ electrodes were prepared using an electrophoretic deposition process. A field of 15 V cm^{-1} was applied to deposit Pd nanostructures using a FTO counter electrode held at positive potentials relative to the working electrode ($BiVO_4$ electrode). For the preparation process of Pd NP-decorated $BiVO_4$ (NP-$BiVO_4$) and Pd NR-decorated $BiVO_4$ (NR-$BiVO_4$) electrodes, the depositing time are 3 and 1 min, respectively. To prepare Pd NP- and NR-decorated $BiVO_4$ (NP-NR-$BiVO_4$) electrodes, Pd NRs were firstly deposited onto the surface of $BiVO_4$ for 30 s and then Pd NPs were deposited for 90 s. After this deposition process, Pd nanostructure-decorated $BiVO_4$ electrodes were rinsed by distilled water and then dried under atmospheric environment for 2 h.

Characterization

X-ray diffraction (XRD) was carried out using a Bruker AXS D8 Advance powder X-ray diffractometer with a Cu Kα (λ = 1.5418 Å) radiation source to confirm the purity and crystallinity of the prepared $BiVO_4$ electrodes. UV-vis spectra were obtained using a Cary 5000 UV-vis-NIR spectrophotometer in diffuse reflectance mode. Scanning electron microscopy (SEM) images were collected with a field-emission SEM (Hitachi Situation-4800). Elemental compositions were determined by Energy Dispersive X-

ray Spectroscopy (EDX) using the EDX detector on the Hitachi Situation-4800. Transmission electron microscopy (TEM) images were obtained with a JEOL 2100F at an accelerating voltage of 200 kV.

Photoelectrochemical Measurements

All photoelectrochemical measurements were carried out in a 0.1-M potassium phosphate buffer (KPi) at pH = 7, using a three-electrode setup, with a Ag/AgCl (4 M KCl) as reference electrode and a platinum foil as counter electrode. Linear scanning voltammograms (LSVs) were obtained with a scan rate of 10 mV s^{-1}. White-light photocurrent measurements were conducted under simulated AM 1.5G solar illumination with a Xe lamp coupled with a Newport Sol3A Class AAA solar simulator (94023A-SR3). The light intensity of the solar light simulator was calibrated to 100 mW cm^{-2} by the standard reference of a Newport 91150 silicon solar cell. Visible (400–800 nm, 98.7 mW cm^{-2}) and NIR (800–2000 nm, 363 mW cm^{-2}) light measurements were conducted with this Xe lamp couple with spectral filters. Monochromatic photocurrent measurements were conducted with this Xe lamp coupled with a set of monochromatic filters. The whole working electrode was illuminated through the back side of FTO glass. The potential vs Ag/AgCl (4 M KCl) can be converted against the reversible hydrogen electrode (RHE) using the following equation:

$$E(\text{vs RHE}) = E(\text{vs Ag/AgCl}) + E_{\text{Ag/AgCl}}(\text{ref}) + 0.0591\text{pH}$$

$$\left(E_{\text{Ag/AgCl}}(\text{ref}) = 0.1976\ \text{V vs RHE at } 25^{\circ}\text{C}\right)$$

Results and Discussion

Figure 1a shows XRD pattern of the $BiVO_4$ film, which can be matched to monoclinic $BiVO_4$ (JCPDS No. 14–0688). In addition, UV-vis absorption spectrum of the $BiVO_4$ film was collected and its bandgap was estimated to be 2.5 eV, which agrees well with values for the bandgap of $BiVO_4$ reported in the literature [19] (Fig. 1b).

Figure 2 shows SEM image and EDX maps of as-prepared NP-NR-$BiVO_4$ composite film and TEM images of Pd nanostructures. SEM image demonstrates that the $BiVO_4$ film is composed of grains with no obvious feature. Although no Pd NPs and NRs can be observed in the SEM image due to their small size (Fig. 2f, g), EDX maps clearly show that Pd element presents a uniform distribution on the surface of $BiVO_4$ film, with the Pd/Bi weight percentage being 2.17 %, indicating that Pd NPs and NRs are successfully decorated on the surface of $BiVO_4$ film. EDX analyses for NP-$BiVO_4$ and NR-$BiVO_4$ electrodes show that the Pd/Bi weight percentages are 2.15 and 1.9 %, respectively.

Figure 3a shows linear scanning voltammograms (LSVs) of NP-$BiVO_4$ and bare $BiVO_4$ electrodes recorded in 1-M KPi solution in the dark and under AM 1.5G illumination (100 mW cm^{-2}). The dark scans collected in the potential range between −0.4 and 0.8 V reveal a small background current of ~10^{-7} A/cm^2. Under AM 1.5G illumination, NP-$BiVO_4$ and bare $BiVO_4$ electrodes show a steady increase in photocurrent with applied potential. Importantly, NP-$BiVO_4$ electrodes exhibited substantially larger photocurrent density than bare $BiVO_4$ electrodes. The photocurrent density is ca. 0.336 mA cm^{-2} at 0.6 V on NP-$BiVO_4$ electrode, which is about 3.3 times higher than that on bare $BiVO_4$ electrode. Furthermore, chronoamperometric curves were collected during a period of 1 h at 0.3 V under AM 1.5G illumination. As shown in Fig. 3b, during such a relatively long period, the enhancement is still noticeable, suggesting that the photoactivity of $BiVO_4$ electrodes can be enhanced under simulated solar light illumination by decoration of Pd NPs on the surface.

Figure 3c shows LSVs of bare $BiVO_4$ and NP-$BiVO_4$ electrodes collected in the potential range from 0.2 to

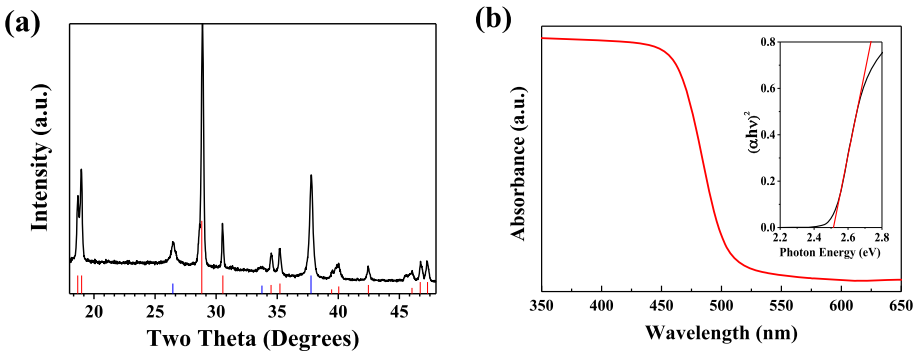

Fig. 1 **a** XRD pattern of the $BiVO_4$ film. The *vertical lines* indicate JCPDS diffraction peaks of FTO (*blue*) and monoclinic $BiVO_4$ (*red*) and **b** UV-vis absorption spectrum of the $BiVO_4$ film. *Inset* shows a Tauc plot of $BiVO_4$ for direct bandgap

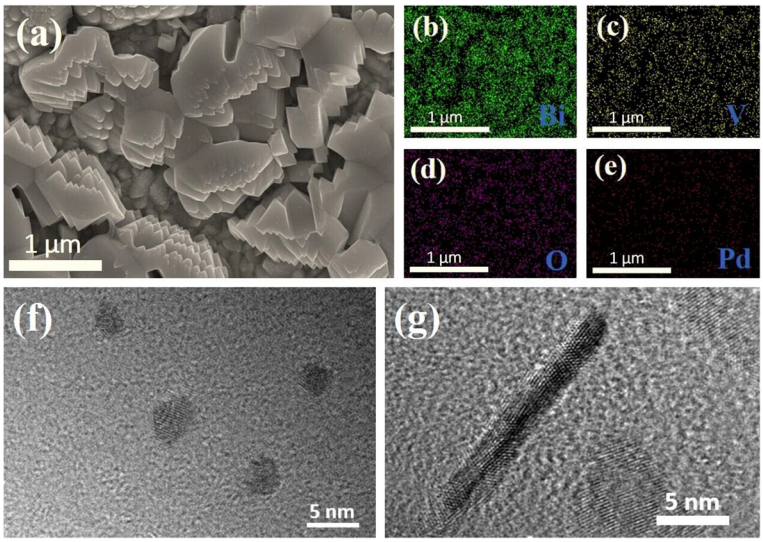

Fig. 2 **a** Typical SEM image and **b**–**e** EDX maps of NP-NR-$BiVO_4$ film for four elements. TEM images of Pd **f** NPs and **g** NRs

1.4 V under dark condition. There is a decrease in current on NP-$BiVO_4$ electrode in the potential ranges between 1.1 and 1.4 V, which could rule out the catalytic effect of Pd NPs on water splitting. Such a current decrease could be ascribed to the fact that the coverage of Pd NPs on the surface of $BiVO_4$ reduces the interfacial surface area between $BiVO_4$ and the electrolyte, and thereby hindering the water oxidation.

To explore the possible reason for the enhanced PEC water splitting on the NP-$BiVO_4$ electrodes, chronoamperometric curves were collected for bare $BiVO_4$ and NP-$BiVO_4$ electrodes under a set of monochromatic light illumination in the visible region. Figure 4a shows the photocurrent response of PEC water splitting on $BiVO_4$ with and without the decoration of Pd NPs under 500 nm (60 mW cm^{-2}) illumination, where the photocurrent on NP-$BiVO_4$ is ca. 4 times of that on pristine $BiVO_4$ electrode. The enhancement factor of photocurrent on the NP-$BiVO_4$ electrode as a function of excitation wavelength was imposed on the absorption spectrum of synthesized Pd NPs stock solution, as shown in Fig. 4b. It can be seen that the enhancement factor strongly depends on the excitation wavelength and that it exhibits a similar trend with Pd NPs absorption spectral feature. Since the Pd absorption spectrum is a consequence of the SPR of Pd NPs, the result suggests that the Pd SPR could be responsible for the observed photocurrent enhancement [24]. Additionally, the photoresponses of bare $BiVO_4$ and NP-$BiVO_4$ electrodes under NIR illumination are obtained and shown in Fig. 4c. The photocurrent collected from NP-$BiVO_4$ electrode slightly decreases in NIR region in comparison with $BiVO_4$ electrode. This result is reasonable since the SPR feature of Pd NPs is located at 573 nm, which is far away from NIR region, and the SPR excitation of Pd NPs cannot occur under NIR illumination.

To extend the photoresponse to NIR region for the PEC water splitting, Pd NRs were decorated on the surface of $BiVO_4$ because the SPR featured peak is located at ca.

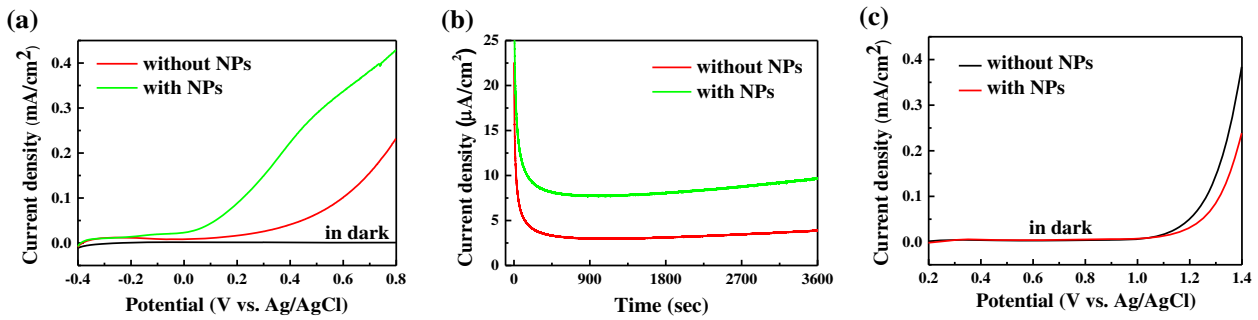

Fig. 3 PEC performance of bare $BiVO_4$ and NP-$BiVO_4$ electrodes: **a** LSVs in the dark and under AM 1.5G illumination, **b** *I*–*t* curves under AM 1.5G illumination at 0.3 V, and **c** LSV in the potential range from 0.2 to 1.4 V under dark condition

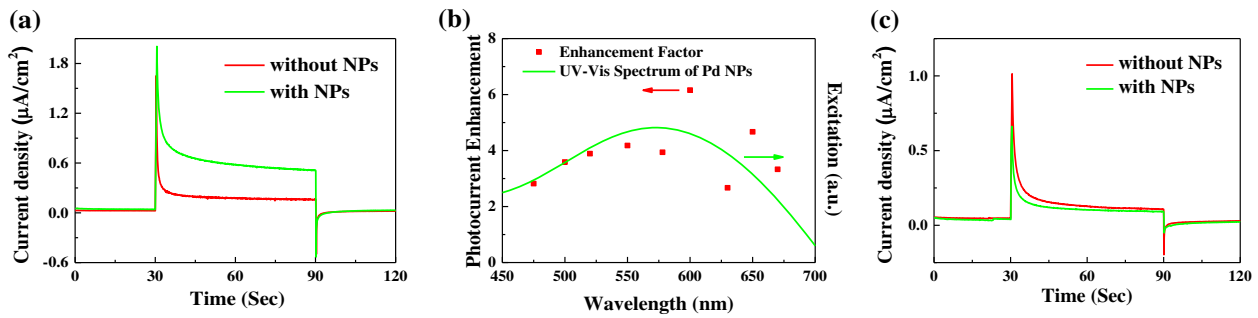

Fig. 4 *I–t* curves at 0.4 V for bare $BiVO_4$ and NP-$BiVO_4$ electrodes under **a** monochromatic light (500 nm) and **c** NIR light illumination. **b** *Symbols*: photocurrent enhancement for NP-$BiVO_4$ electrode as a function of excitation wavelength. *Solid curve*: absorption spectrum of the Pd NPs stock solution

900 nm (see Fig. 5a). Figure 5b–d displays the PEC properties of NR-$BiVO_4$ and bare $BiVO_4$ electrodes. As shown in Fig. 5b, the photocurrent density of NR-$BiVO_4$ electrode under AM 1.5G illumination decreased dramatically compared to bare $BiVO_4$ electrode. The photocurrent density on the NR-$BiVO_4$ and $BiVO_4$ electrodes at 0.6 V are 42 and 146 μA cm^{-2}, respectively. To reveal the plasmonic effect of Pd NRs on the photoresponse of $BiVO_4$ electrodes, photocurrent response for the NR-$BiVO_4$ and bare $BiVO_4$ electrodes was conducted under visible light and NIR light illumination, respectively. As shown in Fig. 5c, the photocurrent for the NR-$BiVO_4$ electrode obtained under visible light illumination greatly decreased relative to bare $BiVO_4$ electrode. Intriguingly, NR-$BiVO_4$ electrode exhibited much enhanced photoactivity under NIR light illumination, as shown in Fig. 5d, indicating that the SPR excitation of Pd NRs is responsible for the enhanced photoactivity of NR-$BiVO_4$ electrodes under NIR light illumination. To the best of our knowledge, this is the first report that the photoactivity of $BiVO_4$ for water splitting can be enhanced in the NIR region by loading plasmonic metal nanostructures [31–33]. As for the

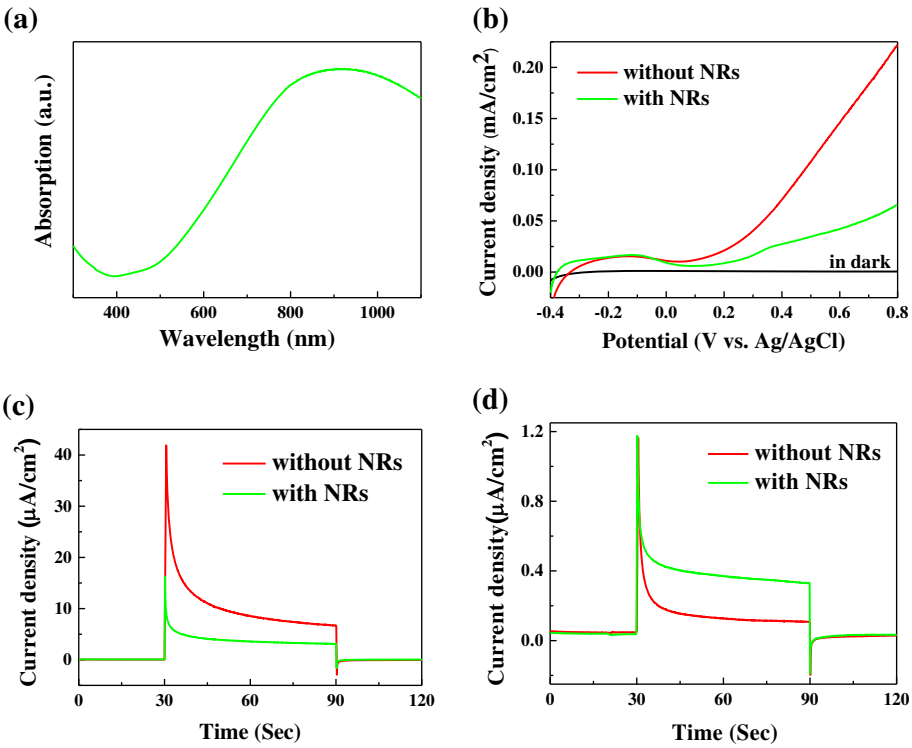

Fig. 5 **a** UV-vis absorption spectrum of Pd NR stock solution. PEC performance of bare $BiVO_4$ and NR-$BiVO_4$ electrodes: **b** LSVs in the dark and under AM 1.5G illumination; *I–t* curves at 0.4 V with **c** visible light and **d** NIR light illumination

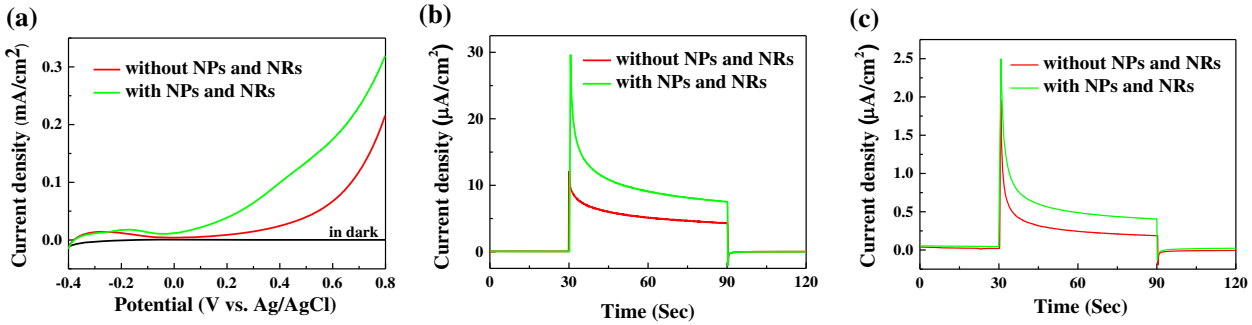

Fig. 6 PEC performance of bare $BiVO_4$ and NP-NR-$BiVO_4$ electrodes: **a** LSVs in the dark and under AM 1.5G illumination; *I–t* curves collected at 0.4 V with **b** visible light and **c** NIR light illumination

photocurrent decrease under visible light and AM 1.5G illumination, it could be attributed to the fact that the presence of Pd NRs not only block the light absorption of $BiVO_4$ but reduce the interfacial surface area between $BiVO_4$ and the electrolyte, thus hindering the transfer of photoexcited holes into the interface between $BiVO_4$ and the electrolyte for water oxidation.

Inspired by the facts that the NP-$BiVO_4$ and NR-$BiVO_4$ electrodes exhibit respectively enhanced PEC water splitting efficiency in the visible and NIR region, a combination of Pd NPs and Pd NRs with $BiVO_4$ electrodes was fabricated by decorating a mixture of Pd NPs and NRs onto the surface of $BiVO_4$ electrode. Figure 6 shows the PEC properties of NP-NR-$BiVO_4$ and bare $BiVO_4$ electrodes. As shown in Fig. 6a, NP-NR-$BiVO_4$ electrode exhibited an enhanced photocurrent density in the potential range from 0.0 to 0.8 V. Importantly, chronoamperometric curves collected under visible and NIR light illumination as shown in Fig. 6b, c demonstrate that the NP-NR-$BiVO_4$ electrode exhibited an enhanced PEC water splitting efficiency in both visible and NIR regions. Although the enhancement factors are not high enough, there must be an optimal loading for Pd NPs and NRs on the $BiVO_4$ to achieve much better PEC performance. Nevertheless, this study is beyond the scope of the current work.

There are three energy transfer mechanisms by which SPR can enhance the concentration of charge carriers in a nearby semiconductor and therefore increase the photocurrent in a PEC cell. These mechanisms include resonant photon scattering, plasmon resonance energy transfer (PRET), and hot electron injection. First, the mechanism of resonant photon scattering can be ruled out for Pd nanostructure-decorated-$BiVO_4$ electrodes containing Pd NPs with the diameter around 3.5 nm and

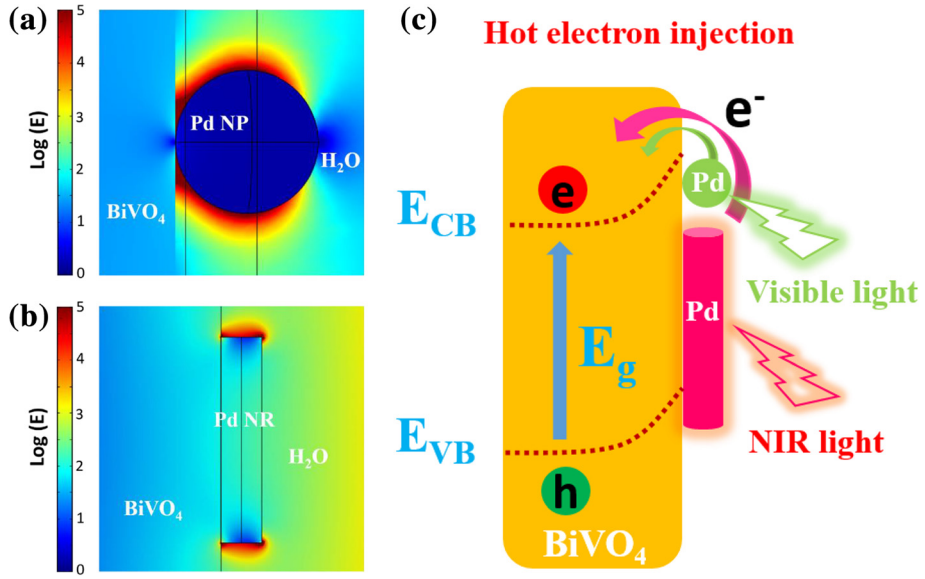

Fig. 7 Spatial distribution of electric-field for **a** NP-$BiVO_4$ and **b** NR-$BiVO_4$ with excitation wavelengths of 500 and 900 nm, respectively. The incident light is along a specific direction (z axis). **c** Schematic illustration of the plasmon-induced charge carrier transfer under visible or NIR light illumination at Pd/$BiVO_4$ interface

Pd NRs with length and width of 11.8 and 1.3 nm, respectively, because it normally occurs in plasmonic metal nanostructures larger than 50 nm in size [34–36]. Second, the effect of PRET is normally observed at wavelengths where the plasmon resonance and semiconductor absorption overlap [37]. Whereas, the SPR feature of Pd NPs and NRs is located at 573 and 900 nm, respectively, indicating that there is barely no absorption overlap between Pd nanostructures and $BiVO_4$ with an absorption band edge around 520 nm. Thus, the effect of PRET can also be ruled out for Pd nanostructure-decorated-$BiVO_4$ electrodes. Third, the hot electron injection from plasmonic metal nanostructures into the conduction band of semiconductors is another possible process following the SPR excitation [38, 39]. Considering that the hot electrons accompany with an enhanced localized electric-field intensity in the vicinity of plasmonic metal nanostructures, the finite-difference time domain (FDTD) simulation was performed to calculate the spatial distribution of local electric-field intensity at the interface between Pd nanostructures and $BiVO_4$ as a function of the wavelength of incident photons. Figure 7a, b shows typical FDTD simulation for Pd NP-$BiVO_4$ and Pd NR-$BiVO_4$ at excitation wavelengths of 500 and 900 nm, respectively. One can clearly observe that the electric-field intensity in the vicinity of Pd NP and Pd NR was greatly enhanced, indicating that there are substantial energetic hot electrons. Thus, in the present work, the hot electron injection mechanism could be the major contributor to the enhanced PEC performance of the Pd nanostructures decorated-$BiVO_4$ electrodes in both visible and NIR regions. As schematically presented in Fig. 7c, under visible or NIR light illumination, Pd NP or NR acts as a sensitizer, absorbing resonant photons, generating the energetic hot electrons from the SPR excitation. Then, the hot electrons pass over the Schottky barrier at the Pd/$BiVO_4$ interface and inject into the conduction band of $BiVO_4$. Schottky barrier at the interface also helps the transferred hot electrons accumulate in the conduction band of $BiVO_4$, preventing them from traveling back to the Pd nanostructures [32, 40].

Conclusions

The photoactivity of Pd NPs and NRs decorated $BiVO_4$ electrodes for PEC water splitting can be effectively enhanced across the visible-NIR region. The enhanced photoactivity in both visible and NIR regions was ascribed to the hot electron injection upon SPR excitation of Pd NPs and NRs, respectively. The present work aimed at enhancing the photoactivity of $BiVO_4$ electrodes and at extending from the visible to the NIR region inspired us to design other plasmonic metal nanostructure-decorated semiconductor photoelectrodes for more effective utilization of the solar spectrum.

Abbreviations

EDX, energy dispersive X-ray spectroscopy; FDTD, finite-difference time domain; LSVs, linear scanning voltammograms; NIR, near-infrared; NP-$BiVO_4$, Pd NPs decorated $BiVO_4$; NP-NR-$BiVO_4$, Pd NPs and NRs decorated $BiVO_4$; NPs, nanoparticles; NR-$BiVO_4$, Pd NRs decorated $BiVO_4$; NRs, nanorods; OECs, oxygen evolution catalysts; PEC, photoelectrochemical; PRET, plasmon resonance energy transfer; SEM, scanning electron microscopy; SPR, surface plasmon resonance; TEM, transmission electron microscopy; XRD, X-ray diffraction.

Competing Interests

The authors declare that they have no competing interests.

Authors' Contributions

WWY carried out the experiments and drafted the manuscript. YJX participated in the experimental design and the statistical analysis. LLZ and ZQZ helped to revise the manuscript. DDL and QXM participated in the coordination and discussion of the study. YSW performed the FDTD simulation. Hui Yang supervised the whole work. All authors have read and approved the final manuscript.

Acknowledgements

We would like to thank the National Basic Research Program of China (973 Program) (2012CB932800) and the National Natural Science Foundation of China (21533005).

Author details

[1]Shanghai Advanced Research Institute, Chinese Academy of Sciences, Shanghai 201210, China. [2]University of Chinese Academy of Sciences, Beijing 100039, China. [3]School of Physical Science and Technology, ShanghaiTech University, Shanghai 201210, China.

Received: 9 March 2016 Accepted: 18 May 2016
Published online: 04 June 2016

References

1. Fujishima A, Honda K (1972) Electrochemical photolysis of water at a semiconductor electrode. Nature 238:37–38
2. Zou ZG, Ye JH, Sayama K, Arakawa H (2001) Direct splitting of water under visible light irradiation with an oxide semiconductor photocatalyst. Nature 414:625–627
3. Chen XB, Shen SH, Guo LJ, Mao SS (2010) Semiconductor-based photocatalytic hydrogen generation. Chem Rev 110:6503–6570
4. Qiu YC, Leung S-F, Wei ZH, Lin QF, Zheng XL, Zhang YG, Fan ZY, Yang SH (2014) Enhanced charge collection for splitting of water enabled by an engineered three-dimensional nanospike array. J Phys Chem C 118:22465–22472
5. Qiu YC, Leung SF, Zhang QP, Hua B, Lin QF, Wei ZH, Tsui KH, Zhang YG, Yang SH, Fan ZY (2014) Efficient photoelectrochemical water splitting with ultrathin films of hematite on three-dimensional nanophotonic structures. Nano Lett 14:2123–2129
6. Park Y, McDonald KJ, Choi K-S (2013) Progress in bismuth vanadate photoanodes for use in solar water oxidation. Chem Soc Rev 42:2321–2337
7. Zhong DK, Choi S, Gamelin DR (2011) Near-complete suppression of surface recombination in solar photoelectrolysis by "Co-Pi" catalyst-modified W: $BiVO_4$. J Am Chem Soc 133:18370–18377
8. Ye H, Park HS, Bard AJ (2011) Screening of electrocatalysts for photoelectrochemical water oxidation on W-doped $BiVO_4$ photocatalysts by scanning electrochemical microscopy. J Phys Chem C 115:12464–12470
9. Pilli SK, Furtak TE, Brown LD, Deutsch TG, Turner JA, Herring AM (2011) Cobalt-phosphate (Co-Pi) catalyst modified Mo-doped $BiVO_4$ photoelectrodes for solar water oxidation. Energy Environ Sci 4:5028–5034
10. Ye H, Lee J, Jang JS, Bard AJ (2010) Rapid screening of $BiVO_4$-based photocatalysts by scanning electrochemical microscopy (SECM) and studies of their photoelectrochemical properties. J Phys Chem C 114:13322–13328
11. Luo WJ, Yang ZS, Li ZS, Zhang JY, Liu JG, Zhao ZY, Wang ZQ, Yan SC, Yu T, Zou ZG (2011) Solar hydrogen generation from seawater with a modified $BiVO_4$ photoanode. Energy Environ Sci 4:4046–4051
12. Jo WJ, Jang J, Kong K, Kang HJ, Kim JY, Jun H, Parmar KPS, Lee JS (2012) Phosphate doping into monoclinic $BiVO_4$ for enhanced photoelectrochemical water oxidation activity. Angew Chem Int Ed 51:3147–3151

13. McDonald KJ, Choi KS (2012) A new electrochemical synthesis route for a BiOI electrode and its conversion to a highly efficient porous $BiVO_4$ photoanode for solar water oxidation. Energy Environ Sci 5:8553–8557
14. Su J, Guo L, Yoriya S, Grimes CA (2010) Aqueous growth of pyramidal-shaped $BiVO_4$ nanowire arrays and structural characterization: application to photoelectrochemical water splitting. Cryst Growth Des 10:856–861
15. He HC, Berglund SP, Rettie AJE, Chemelewski WD, Xiao P, Zhang YH, Mullins CB (2014) Synthesis of $BiVO_4$ nanoflake array films for photoelectrochemical water oxidation. J Mater Chem A 2:9371–9379
16. Yoon H, Mali MG, Choi JY, Kim MW, Choi SK, Park H, Al-Deyab SS, Swihart MT, Yarin AL, Yoon SS (2015) Nanotextured pillars of electrosprayed bismuth vanadate for efficient photoelectrochemical water splitting. Langmuir 31:3727–3737
17. Rao PM, Cai LL, Liu C, Cho IS, Lee CH, Weisse JM, Yang PD, Zheng XL (2014) Simultaneously efficient light absorption and charge separation in WO_3/$BiVO_4$ core/shell nanowire photoanode for photoelectrochemical water oxidation. Nano Lett 14:1099–1105
18. Su JZ, Guo LJ, Bao NZ, Grimes CA (2011) Nanostructured WO_3/$BiVO_4$ heterojunction films for efficient photoelectrochemical water splitting. Nano Lett 11:1928–1933
19. Seabold JA, Choi K-S (2012) Efficient and stable photo-oxidation of water by a bismuth vanadate photoanode coupled with an iron oxyhydroxide oxygen evolution catalyst. J Am Chem Soc 134:2186–2192
20. Wang DE, Li RG, Zhu J, Shi JY, Han JF, Zong X, Li C (2012) Photocatalytic water oxidation on $BiVO_4$ with the electrocatalyst as an oxidation cocatalyst: essential relations between electrocatalyst and photocatalyst. J Phys Chem C 116:5082–5089
21. Cho S, Lee MJ, Kim MS, Lee S, Kim YK, Lee DH, Lee CW, Cho KH, Chung JH (2008) Infrared plus visible light and heat from natural sunlight participate in the expression of MMPs and type I procollagen as well as infiltration of inflammatory cell in human skin in vivo. J Dermatol Sci 50:123–133
22. Zhang ZH, Zhang LB, Hedhili MN, Zhang HN, Wang P (2013) Plasmonic gold nanocrystals coupled with photonic crystal seamlessly on TiO_2 nanotube photoelectrodes for efficient visible light photoelectrochemical water splitting. Nano Lett 13:14–20
23. Pu YC, Wang G, Chang KD, Ling Y, Lin YK, Fitzmorris BC, Liu CM, Lu X, Tong Y, Zhang JZ, Hsu YJ, Li Y (2013) Au nanostructure-decorated TiO_2 nanowires exhibiting photoactivity across entire UV-visible region for photoelectrochemical water splitting. Nano Lett 13:3817–3823
24. Ingram DB, Linic S (2011) Water splitting on composite plasmonic-metal/semiconductor photoelectrodes: evidence for selective plasmon-induced formation of charge carriers near the semiconductor surface. J Am Chem Soc 133:5202–5205
25. Xu Z, Lin YY, Yin M, Zhang HF, Cheng CW, Lu LF, Xue XZ, Fan HJ, Chen XY, Li DD (2015) Understanding the enhancement mechanisms of surface plasmon-mediated photoelectrochemical electrodes: a case study on Au nanoparticle decorated TiO_2 nanotubes. Adv Mater Interfaces 2:1500169
26. Jain PK, El-Sayed MA (2008) Noble metal nanoparticle pairs: effect of medium for enhanced nanosensing. Nano Lett 8:4347–4352
27. Malinsky MD, Kelly KL, Schatz GC, Van Duyne RP (2001) Chain length dependence and sensing capabilities of the localized surface plasmon resonance of silver nanoparticles chemically modified with alkanethiol self-assembled monolayers. J Am Chem Soc 123:1471–1482
28. Haes AJ, Van Duyne RP (2002) A nanoscale optical biosensor: sensitivity and selectivity of an approach based on the localized surface plasmon resonance spectroscopy of triangular silver nanoparticles. J Am Chem Soc 124:10596–10604
29. Xiong YJ, Wiley B, Chen JY, Li ZY, Yin YD, Xia YN (2005) Corrosion-based synthesis of single-crystal Pd nanoboxes and nanocages and their surface plasmon properties. Angew Chem Int Ed Engl 44:7913–7917
30. Liu YT, Xu Z, Yin M, Fan HW, Cheng WJ, Lu LF, Song Y, Ma J, Zhu XF (2015) Enhanced photoelectrocatalytic performance of alpha-Fe_2O_3 thin films by surface plasmon resonance of Au nanoparticles coupled with surface passivation by atom layer deposition of Al_2O_3. Nanoscale Res Lett 10:374
31. Zhang LW, Lin CY, Valev VK, Reisner E, Steiner U, Baumberg JJ (2014) Plasmonic enhancement in $BiVO_4$ photonic crystals for efficient water splitting. Small 10:3970–3978
32. Zhang LW, Herrmann LO, Baumberg JJ (2015) Size dependent plasmonic effect on $BiVO_4$ photoanodes for solar water splitting. Sci Rep 5:16660
33. Abdi FF, Dabirian A, Dam B, van de Krol R (2014) Plasmonic enhancement of the optical absorption and catalytic efficiency of $BiVO_4$ photoanodes decorated with Ag@SiO_2 core-shell nanoparticles. Phys Chem Chem Phys 16:15272–15277
34. Evanoff DD, Chumanov G (2005) Synthesis and optical properties of silver nanoparticles and arrays. ChemPhysChem 6:1221–1231
35. Burda C, Chen XB, Narayanan R, El-Sayed MA (2005) Chemistry and properties of nanocrystals of different shapes. Chem Rev 105:1025–1102
36. Kelly KL, Coronado E, Zhao LL, Schatz GC (2003) The optical properties of metal nanoparticles: the influence of size, shape, and dielectric environment. J Phys Chem B 107:668–677
37. Warren SC, Thimsen E (2012) Plasmonic solar water splitting. Energy Environ Sci 5:5133–5146
38. Linic S, Christopher P, Ingram DB (2011) Plasmonic-metal nanostructures for efficient conversion of solar to chemical energy. Nat Mater 10:911–921
39. Tian Y, Tatsuma T (2005) Mechanisms and applications of plasmon-induced charge separation at TiO_2 films loaded with gold nanoparticles. J Am Chem Soc 127:7632–7637
40. Qian K, Sweeny BC, Johnston-Peck AC, Niu WX, Graham JO, DuChene JS, Qiu JJ, Wang YC, Engelhard MH, Su D, Stach EA, Wei WD (2014) Surface plasmon-driven water reduction: gold nanoparticle size matters. J Am Chem Soc 136:9842–9845